Formation of Hot Cracks in Austenitic Stainless Steel Welds—Solidification Cracking

Crack formation is controlled by phase transformations and interfacial energy considerations

BY V. P. KUJANPÄÄ, S. A. DAVID AND C. L. WHITE

ABSTRACT. Solidification cracking in austenitic stainless steel welds was investigated by Spot-Varestraint tests using pure laboratory heats and commercial heats. The initiation and propagation of solidification cracks were found to be controlled by the formation of the solidification grain boundary, interfacial energy considerations, and the phase transformations occurring upon solidification. The ability to backfill the cracks also affects the extent of cracking observed in welds. The primary austenitic mode of solidification occurring in some of these alloys enables cracks to initiate and propagate more easily. This is further enhanced by sulfur segregation. The primary ferritic mode of solidification, however, inhibits crack initiation and propagation and promotes backfilling.

Introduction

Hot cracking in austenitic stainless steels is one of the most investigated areas in welding. A number of papers related to this subject have been published in the last few decades (Refs. 1–11). Over the years, several important observations have been made, and valuable relationships between significant variables and hot-cracking susceptibility have been drawn. It is generally known that impurities, such as sulfur and phosphorus, can increase susceptibility to cracking. Delta ferrite, in amounts between 5 and 20% in the room temperature microstructure, also prevents hot cracking in many austenitic stainless steels (Refs. 12–15). Recently, this relationship has been found to be related to the mode of solidification, *i.e.*, primary ferritic mode of solidification providing the best resistance to hot cracking (Refs. 16–20). The high hot-cracking susceptibility of welds solidifying in a primary austenitic mode can be minimized by controlling welding process variables or composition (Refs. 21–27); however, this is not always practical. Hot cracking is therefore still a problem requiring more research to understand its mechanisms and to design workable solutions.

Several kinds of elevated temperature cracks have been observed in materials, all of which are known as hot cracks. Hemsworth, *et al.* (Ref. 28), have classified them into two types. Type I, segregation cracks, are formed at temperatures close to the solidus, where a small volume fraction of liquid still exists. Of the various types of segregation cracks, solidification cracking, which occurs during the last stages of solidification, is the most common and most investigated type of segregation cracking. Type II, ductility dip cracks, may occur at lower temperatures in the weldment. These cracks form at newly migrated grain boundaries, and are always free from liquid films.

Although a great deal of work related to hot cracking has been done over the years, none of these investigations has focused on the relationship between hot cracking in high-purity model alloy systems and related commercial austenitic stainless steels. The aim of this work was to investigate the formation of hot cracks in austenitic stainless steel welds, both in the high-purity model and the commercial alloy systems. Auger electron spectroscopy (AES) was used to study the top few atom layers on the hot-cracked surfaces. Although AES has been used in the past to study such surfaces, the results have been confused by extensive contamination of the surfaces by exposure to the laboratory environment during welding, and to coolants, etc., during specimen preparation. In this study, we report AES analyses of internal hot cracks that were exposed by fracturing in the ultra-high-vacuum of the AES analysis chamber, thereby avoiding contamination and the attendant confusion of the results. The observations are related to the mechanism of formation of hot cracks in these welds.

Experimental Procedure

Materials

Alloy compositions were chosen to investigate both the effect of impurities and the mode of solidification on the hot-cracking susceptibility of austenitic stainless steel welds. Both laboratory heats and commercial heats were used. Their compositions are listed in Table 1. Commercial heats were of Types AISI 304, 309, 310 and 316 and one commercial non-AISI type containing 20% Cr, 25% Ni, 6% Mo and 0.2% N, designated AL6XN. Laboratory heats A to E are corresponding ternary Fe-Cr-Ni alloys. These alloys were made using pure zone-refined iron, chromium and nickel. They were arc melted and cast into 25 × 12.5 × 50 mm (1 × ½ × 2 in.) ingots, heat treated in vacuum (1100°C/2012°F, 2 h), hot rolled (50%), heat treated again (1100°C, 2 h) and cold rolled to the final thickness, 4.8 mm (3/16 in.).

Specimens for the Spot-Varestraint test were machined to the dimensions shown in Fig. 1. In the specimens of laboratory heats, only the central part was of the material to be tested. This section was

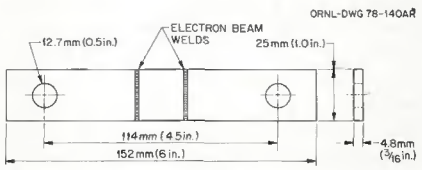

Fig. 1—Dimensions of Spot-Varestraint specimens

V. P. KUJANPÄÄ is a Research Staff Member, Laboratory of Physical Metallurgy, University of Oulu, Oulu, Finland. S. A. DAVID and C. L. WHITE are with the Metals and Ceramics Division, Oak Ridge National Laboratory, Oak Ridge, Tenn.

Table 1—Compositions of Materials Tested (wt-%)

Heat	C	Si	Mn	P	S	Cr	Ni	Mo	Cu	N	Ti	Nb	Cr_{eq}/Ni_{eq}[a]
A	0.004	<0.01	<0.01	0.005	0.007	20.0	16.1	0.02	0.01	0.001	<0.01	<0.01	1.24
B	0.006	<0.01	<0.01	0.005	0.006	19.8	10.9	0.01	<0.01	<0.001	<0.01	<0.01	1.80
C	0.005	<0.01	<0.01	0.005	0.008	26.0	25.4	0.01	0.02	0.001	<0.01	<0.01	1.02
D	0.005	<0.01	<0.01	0.005	0.007	25.7	20.0	0.01	0.02	0.001	<0.01	<0.01	1.28
E	0.006	<0.01	<0.01	0.005	0.007	25.7	15.3	0.01	0.01	0.003	<0.01	<0.01	1.67
304	0.079	0.45	1.67	0.026	0.015	18.6	8.5	0.13	0.17	0.004	<0.01	<0.01	1.77
309	0.020	0.42	2.01	0.015	0.008	23.2	14.2	0.05	0.04	0.029	0.01	<0.01	1.52
310	0.036	0.45	0.96	0.019	0.009	25.7	19.1	0.15	0.25	0.023	0.02	<0.01	1.28
316	0.039	0.29	1.94	0.026	0.012	16.8	11.5	2.33	0.16	0.021	<0.01	<0.01	1.52
AL6XN	0.022	0.43	1.54	0.026	0.007	20.7	24.8	6.24	0.07	0.21	<0.01	<0.01	1.04

[a]Calculated according to Hammar and Svensson (Ref. 38).

electron beam welded to the extension tabs of AISI 304 steel before machining.

Spot-Varestraint Method

The Spot-Varestraint or Tigamajig test (Ref. 29) was developed from the original Varestraint test (Ref. 30). It maintains the desirable features of the original Varestraint test and additionally permits the use of smaller specimens. In this test, the specimen is subjected to a gas tungsten arc spot weld thermal cycle for sufficient time to establish approximately steady-state thermal conditions. As the arc current is interrupted, an augmented strain is applied to the specimen by bending. Depending on the delay between extinguishing the arc and the start of bending, either solidification cracks or HAZ cracks can be formed. An approximate delay time of 0.5 s was used for solidification cracking. The tangential strain on the top surface of the specimen, ϵ, is a function of specimen thickness, t, and bending radius, R, and can be calculated from:

$$\epsilon \approx t/2R \qquad (1)$$

Specimens from each heat were tested at strains from 0.9 to 4.9%. The other variables were kept constant and are shown in Table 2.

Metallography

The test welds were cleaned and examined both visually and by stereo light microscopy. The number and lengths of the cracks were measured on the specimen surface using optical microscopy. In this study, the individual crack lengths are summed up, and the sum is designated as the total crack length (TCL) at a given strain. The metallographic specimens were prepared along a section parallel to the surface of the weld and etched using a solution containing HNO_3 and H_2O. The microstructure was examined under a conventional light microscope, paying special attention to the mode of solidification, the microstructure, and their relation to the cracking tendency. Scanning electron microscopy (SEM) was used to investigate the mode of fracture.

An electron probe microanalyzer (EPMA) at 20 kV with a minimum beam diameter (1 μm) was used to characterize the segregation behavior in the weld metal, and to determine the composition of backfilled cracks. Concentration profiles were obtained by step-scanning technique (step interval 1 μm, sampling time 5 to 30 s) and using a ZAF correction program.

Small tensile specimens containing cracks of interest were cut from tested Spot-Varestraint specimens for analysis using Auger electron spectroscopy. Care was taken to section these specimens so that they would contain internal cracks that were not connected to the external surface. This is necessary in order to avoid contamination of the crack surfaces during welding and by coolants during metallographic sectioning. The tensile specimens were then fractured under a vacuum of the order of 2×10^{-8} Pa in a high-spatial-resolution scanning AES system. Auger spectra were obtained using a 5-keV primary electron beam having a beam current of approximately 0.5 nA. The secondary electron spectrum was detected using pulse-counting techniques, and the $E \cdot N(E)$ versus E spectra were differentiated using a dedicated computer to provide the more familiar derivative-type Auger spectra.

Semiquantitative analysis of Auger spectra involved measuring peak-to-peak intensities in the derivative spectra and correcting peak intensities from different elements, using relative sensitivity factors from published spectra of pure elements and compounds (Ref. 31). These analyses do not correct for effects of chemical interactions and variations in matrix composition, and therefore should be viewed as approximate.

Following AES analysis of as-fractured specimens, the fracture surfaces were sputter etched using Ar ions having an energy of 5 keV. The incident ion current density was 12 $\mu A/cm^2$, and we estimate a removal rate on the order of 3 to 5 atom layers per minute. Alternate AES analysis and sputter etching provided information regarding the depth distribution of segregating elements.

Ferrite numbers of the welds were measured using a Magne-Gage calibrated according to the AWS procedure A4.2-74.

Results and Discussion

Microstructure

The solidification modes of the welds were assessed on the basis of careful examination of their microstructure, paying special attention to the delta ferrite morphology and the etching contour of austenite, according to the procedures presented elsewhere in the literature (Refs. 21–37). The results are shown in Table 3, along with the measured room temperature ferrite numbers.

Figure 2 shows solidification modes, the chromium equivalent, and the nickel equivalent for various alloys used in this investigation. Of the various equivalents cited in literature, those developed by Hammar and Svensson (Ref. 38) were used because they were found best to correlate with the solidification mode (Ref. 39).

Alloys A, C, D, 310 and AL6XN were

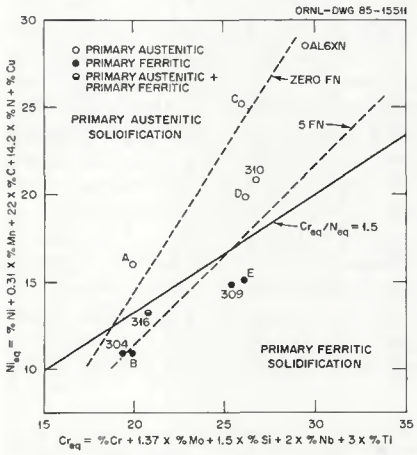

Fig. 2—Compositions of test materials in a chromium equivalent-nickel equivalent diagram, showing fields of solidification modes and constant ferrite lines of room temperature ferrite content

Table 2—Parameters Used in Spot-Varestraint Tests

Method	Gas tungsten arc
Position	Flat
Polarity	DCEN
Current	75 A
Arc length	3.2 mm (⅛ in.)
Electrode	EWTh-2, diam. 2.4 mm (3/32 in.), cone angle 10 deg
Arc time	23 s
Shielding gas	99.99% Ar, flow rate 14 L/min (30 cfh)
Applied strain	0.9, 2.9 or 4.9%

found to exhibit a primary austenitic mode of solidification (A) and Alloys B, E, 304 and 309 exhibited a primary ferritic mode of solidification (FA). The present results are in good agreement with the earlier studies (Ref. 40), showing that the demarcation line between the fields of primary austenitic and primary ferritic solidification modes corresponds to a ratio of chromium-equivalent to nickel-equivalent of about 1.5.

Figure 3A shows the fully austenitic microstructure observed in Alloys A, C and AL6XN, confirming an austenitic mode of solidification. The interdendritic regions appear dark due to the etching effect. No second phase, in particular ferrite, was observed in the microstructure. The major phase in Alloys D and 310 was austenite; however, these alloys contained a small percent of delta ferrite

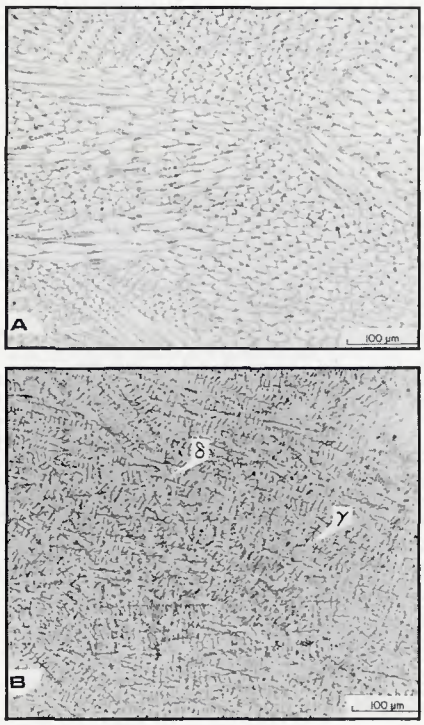

Fig. 3—Microstructures of the welds that solidified in: A—primary austenitic mode (Alloy C); B—primary ferritic mode (Alloy 304)

Table 3—Solidification Modes and Ferrite Contents of the Welds of Different Materials

Material	Solidification Mode[a]	Ferrite Number[b]
A	A	0.0
B	FA	5.2–5.5
C	A	0.0
D	AF	1.5–1.7
E	FA	26–27
304	FA	2.9–3.1
309	FA	12–14
310	AF	1.2–1.4
316	FA(AF)[c]	2.6–2.8
AL6XN	A	0.0

[a]A—single-phase austenitic; AF—austenitic-ferritic; FA—ferritic-austenitic.
[b]Measured by Magne-Gage.
[c]Ten to thirty percent of the grains in the welds had solidified in AF mode.

(1.3 to 1.9 FN) in the interdendritic regions. This indicates that ferrite stabilizing elements partitioned to the liquid, leading to the formation of ferrite during the last stages of solidification. This shows an austenitic-ferritic (AF) mode of solidification for these alloys.

Welds of Alloys B, E, 304 and 309, solidifying in a primary ferritic mode, revealed a duplex $\gamma + \delta$ microstructure, as shown in Fig. 3B. Delta ferrite (3–27 FN) was found to be located mainly in the cores of dendrites, indicating that delta ferrite was the initial phase formed during solidification. Also, the primary ferrite has transformed to austenite through peritectic reaction and subsequent solid-state transformations. This may be classified under the ferritic-austenitic mode of solidification, in contrast to single-phase ferritic solidification, found in duplex steels. The Type 316 stainless steel appeared to exhibit a mixed mode of freezing, with some of the grains solidified in the primary ferritic mode and others in the primary austenitic mode. Between 10 and 30% of the microstructure was estimated to have solidified in the primary austenitic mode.

The solidification substructure of the welds was found to be mostly cellular or cellular dendritic; however, a small fraction of the weld along the periphery contained evidence of planar growth. This observation was most common in the pure laboratory heats. Equiaxed dendritic growth was also observed in the center of some of the spot welds. The cracks, when observed, were predominantly located along the boundaries of grains containing cellular or cellular dendritic structure.

The solidification grain structure in these welds could be revealed by using a suitable etching technique. The grain boundaries were etched more easily in welds exhibiting the primary austenitic solidification mode (Fig. 3A) than in those exhibiting the primary ferritic mode of solidification. A careful examination of the fully austenitic microstructure of the laboratory heats, as shown in Fig. 4, revealed extensive migration of the original solidification boundary during the post-solidification cooling period.

The location of the observed room-temperature grain boundary is entirely different from the solidification boundary, defined by the region separating a group of cells or dendrites of one orientation from the other. This has been clearly shown on the photomicrograph by drawing a discontinuous line through such a boundary—Fig. 4. In certain

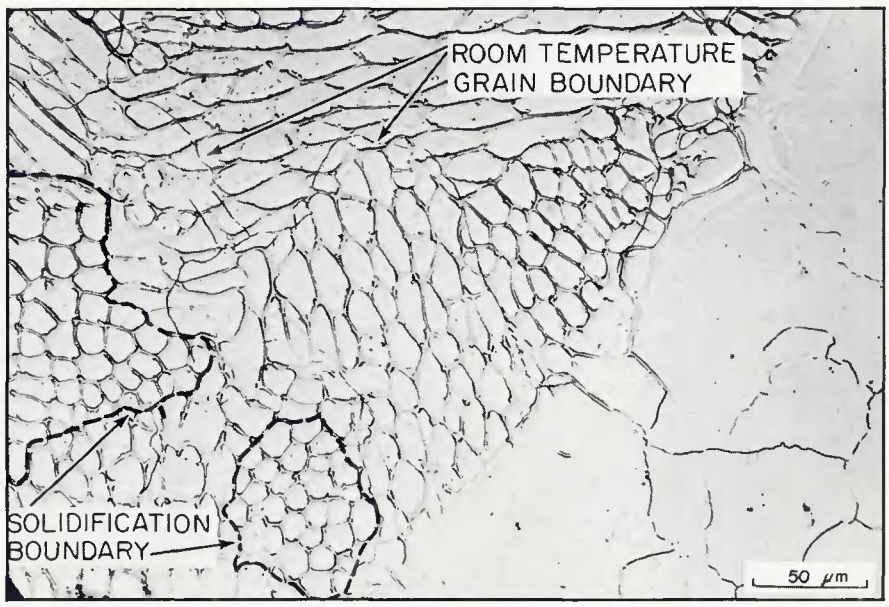

Fig. 4—Location of room temperature grain boundaries with respect to the (outlined) solidification grain boundaries (in Alloy C)

Fig. 5—Location of the solidification cracks in the weld macrostructure

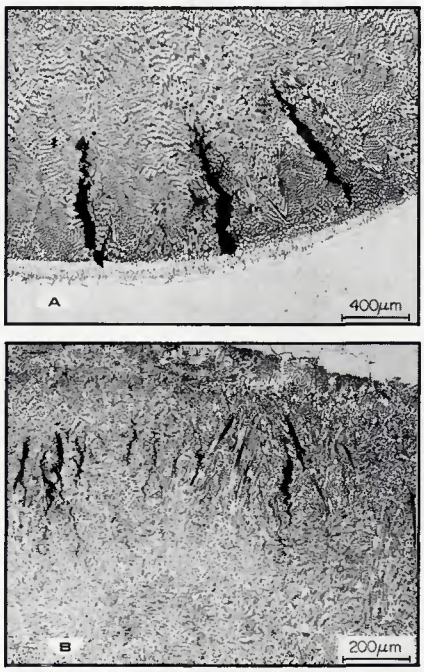

Fig. 6—Location of the solidification cracks in the microstructure of a weld solidified in: A—primary austenitic mode (Alloy A); B—primary ferritic mode (Alloy 304)

regions, the observed grain boundary cuts across several cells. Also, the migration has been found to be more extensive in the pure experimental heats than in commercial heats. Migration of the original solidification boundary may be possible due to the absence of inclusions or second phase (ferrite) to pin the boundaries. Although the exact reason for this migration is not known at the present time, it could be driven by plastic strain induced by residual stresses due to solidification shrinkage and thermal stresses. For welds solidifying in the primary ferritic mode, it was hard to reveal the room-temperature grain boundaries. Even here the original solidification boundary has been found to migrate and get pinned or incorporated into the ferrite-austenite interphase interface. Similar observations have been made by Brooks, *et al.* (Ref. 27), and Gooch, *et al.* (Ref 21).

Solidification Cracks

An examination of the crack surface and the microstructure close to the crack tips indicated the presence of liquid at the time of crack initiation and propagation. Almost all of the cracks were oriented along the solidification direction, and the majority of them were in the region where this direction was normal to the direction of maximum applied strain, as shown in Fig. 5.

Most of the solidification cracks were found to be located on solidification grain boundaries. This was particularly true in the welds that solidified in the primary austenitic mode—Fig. 6. A small number of intragranular cracks were observed; however, they were always interdendritic in nature and present mostly in welds that solidified in the primary ferritic mode. In the welds solidifying in the primary ferritic mode, the location of room temperature grain boundaries had no correlation with the location of solidification cracks.

In Type 316 welds, which exhibited a mixed mode of solidification, most of the cracks were found to be located in a region that had solidified in the primary austenitic mode, as shown in Fig. 7.

Microstructural features indicating backfilling of the cracks were found in a majority of the welds. Backfilling was revealed especially in the welds solidified in a primary ferritic mode—Fig. 8.

Solidification crack surfaces were studied by SEM. The fractographs in Fig. 9 show cellular or cellular dendritic structure, indicating that the crack had formed at elevated temperatures while some liquid was still present.

Susceptibility to Solidification Cracking

Figure 10 shows the dependence of the total crack length on the applied strain. It shows that the level of cracking increases with the applied strain. The minimum strain required for cracking is

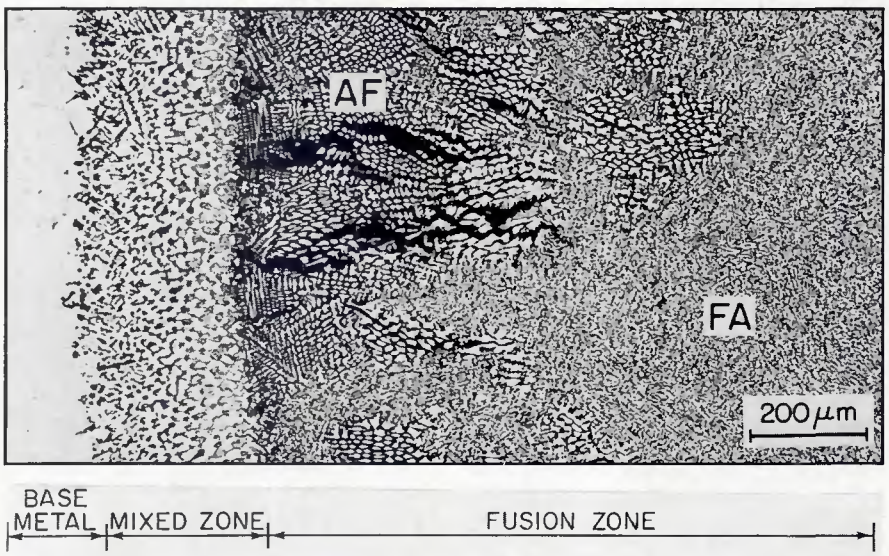

Fig. 7—Location of the solidification cracks in the microstructure of the Type 316 weld, which has regions of primary austenitic (AF) and primary ferritic (FA) solidification

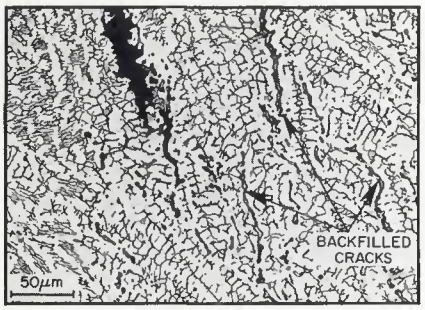

Fig. 8 — Traces of backfilling in Type 304 weld

≤1% for Alloys A, C, 310, 316 and AL6XN; ~2% for Alloy 309, ~3% for Alloys D and 304; and >5% for Alloys B and E.

Figure 10 also shows the influence of solidification mode on solidification cracking. Welds solidifying in a primary austenitic mode seem to be more susceptible to cracking than welds solidifying in a primary ferritic mode. The lone exception seems to be Alloy D, which was less susceptible to cracking than primary ferrite mode Alloy 309. Alloy 316, which solidified in a mixed primary austenitic-primary ferritic mode, exhibited cracks predominantly located in regions that had solidified as primary austenite, which explains its high susceptibility.

It is also evident from Fig. 10 that among the alloys solidifying in primary austenitic mode, there was no remarkable difference between the solidification cracking level of commercial austenitic stainless steels and that of the ternary Fe-Cr-Ni alloys. The welds solidifying in a primary ferritic mode, however, showed clearly a lower tendency toward solidification cracking. Among these welds, the ternary Fe-Cr-Ni heats showed practically no cracks, while some cracks were observed in the commercial heats.

Figure 11 shows the relationship between ferrite number and susceptibility to solidification cracking at an applied strain level of 4.9%. It shows that for ferrite levels ≥3 FN, the cracking tendency is low. This ferrite level corresponds to a composition at which the mode of freezing may change from primary austenitic to primary ferritic mode. The experimental high-purity alloy welds solidifying in primary austenitic mode, in spite of low impurity content, seem to be more susceptible to cracking than welds solidifying in a ferritic mode. Again,

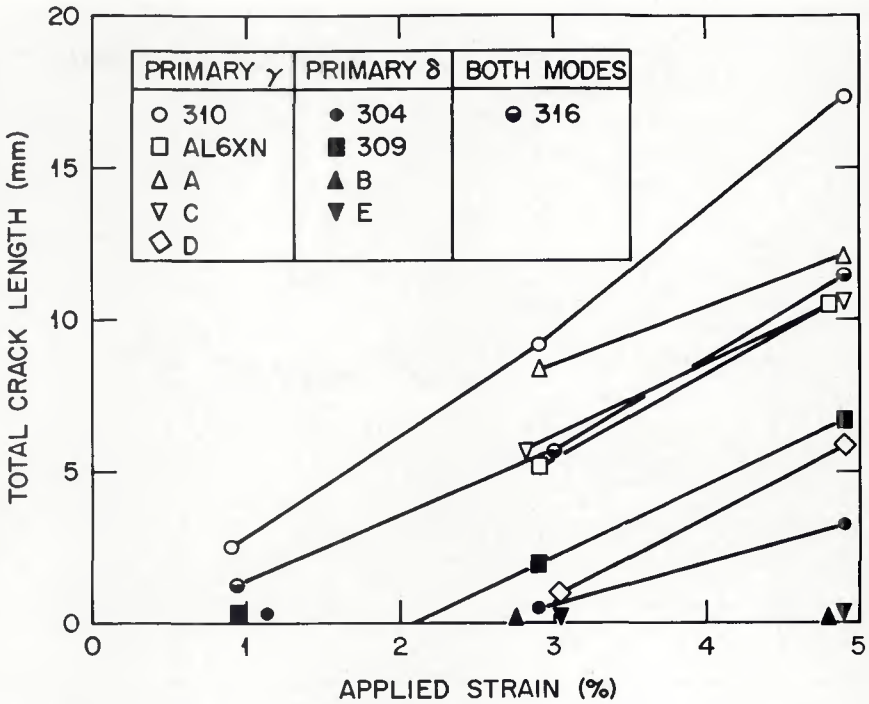

Fig. 10 — Dependence of the total crack length on the applied strain

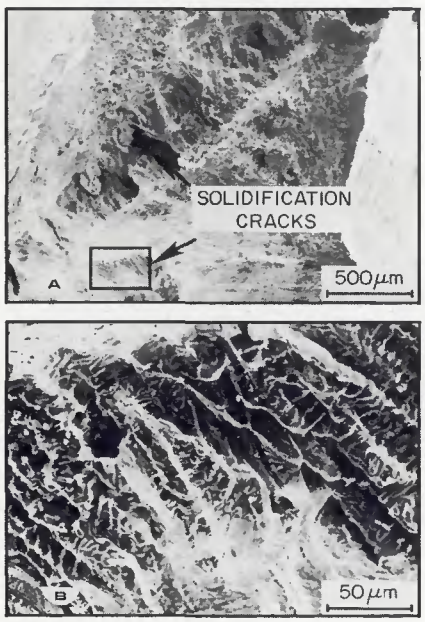

Fig. 9 — Fracture surface of a solidification crack in Type 310 weld. A — Low-magnification image; B — High-magnification image of the surface element shown in A

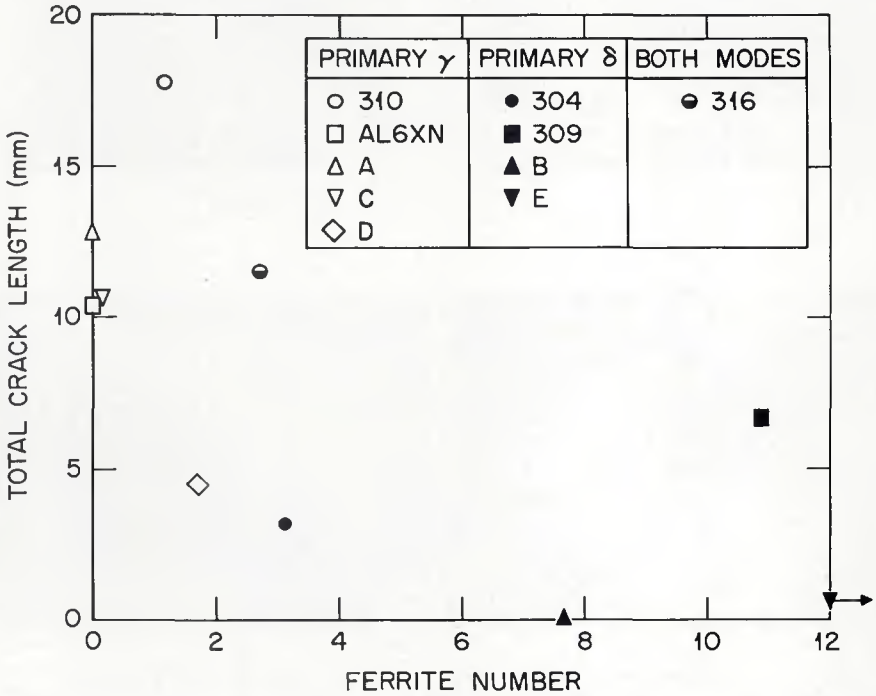

Fig. 11 — Relation between the total crack length and the room temperature ferrite number for the welds (4.9% applied strain)

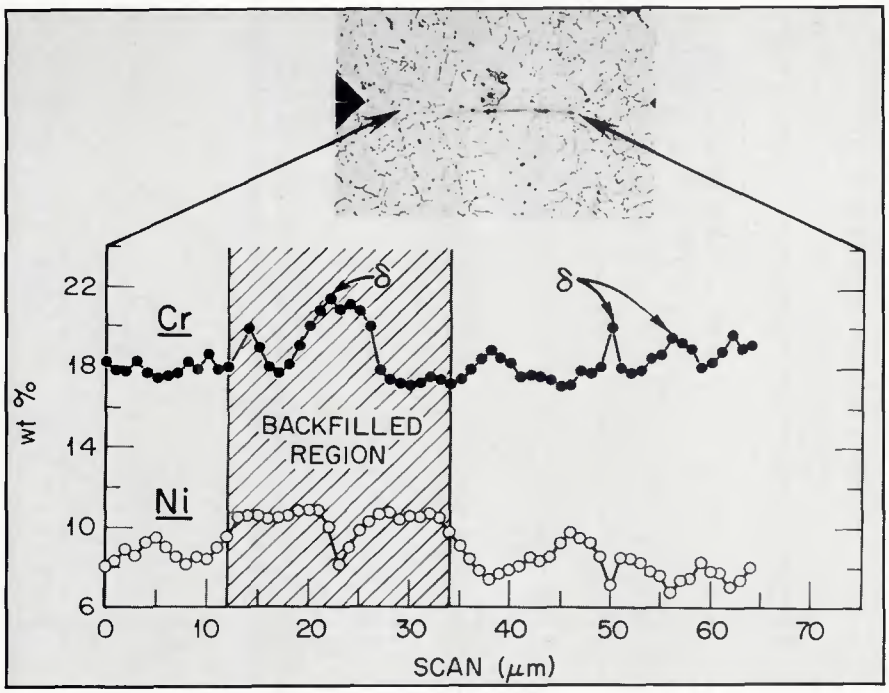

Fig. 12—Step scanning profiles for chromium and nickel in the back-filled regions of the weld

among the welds solidifying in primary ferritic mode, the commercial alloys are more susceptible to cracking than the high-purity experimental alloys.

EPMA and AES Results

The backfilling of cracks was investigated using EPMA. Step scan profiles for chromium and nickel close to the cracks in Weld 304, which solidified in a primary ferritic mode, are shown in Fig. 12. The average nickel composition of the region close to the crack was found to be high. This is because the mode of freezing for this alloy is primary ferritic, and so as the volume fraction of the solid (primary ferrite) increases, the liquid is enriched in nickel. Thus the liquid backfilling in the crack and the subsequent solid that forms in this region is enriched in nickel. This is an evidence of backfilling.

The elemental distribution on the solidification crack surfaces was investigated using AES. Figures 13–16 show typical results for Alloys 310 and C. Scanning electron micrographs of the solidification crack surfaces exposed inside the AES system and the distributions of Fe, Cr, Ni and S (Auger maps) over these fields of view are shown in Figs. 13 and 15. Both elemental maps (Figs. 13 and 15) and Auger spectra (Figs. 14 and 16) show that

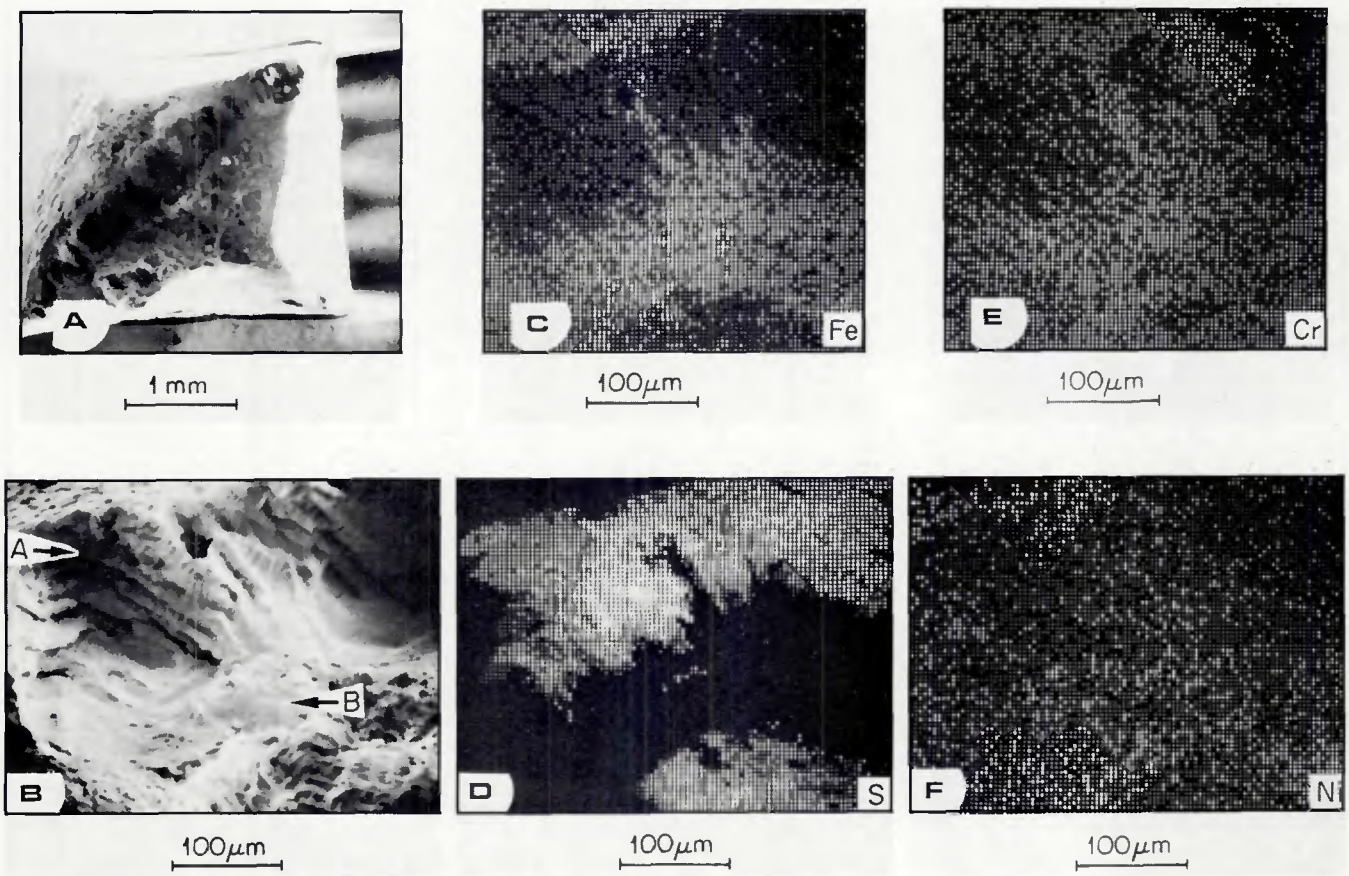

Fig. 13—AES studies on Type 310 weld solidification crack opened inside the Auger electron microscope. A and B—SEM image of the surface studied; C through F—Fe, S, Cr and Ni AES maps, respectively

the solidification crack surfaces were enriched mainly in sulfur; however, the spectra also reveal chromium enrichment, relative to iron, in these regions. The Auger spectrum, taken on the solidification crack surface of Alloy 310, Curve (a), in Fig. 14, revealed a much larger Auger peak from S than did the region of ductile tearing—Curve (c). Similar observations were true for the ternary Alloy C (Figs. 14 and 16). The low levels of C and absence of detectable O indicated in the as-fractured spectra show that the areas analyzed had not been connected to the external surface prior to fracture in the AES system.

Sputter etching and reanalysis of the surfaces in Figs. 13 and 15 revealed that the sulfur-enriched layers on the crack surfaces were of the order of 1 nm thick. The sulfur content on the top layer was estimated to be 20 to 30 at.-%, which is about 2000 times the bulk sulfur composition of the alloys.

Initiation of Solidification Cracks

It is commonly suggested that solidification cracks initiate on the solidification grain boundaries at a temperature close to the solidus, while a small fraction of liquid still exists. It must be emphasized, however, that the grain boundaries can migrate and change their position during post-solidification cooling, as discussed previously.

Figure 17 is a schematic representation of different solidification modes in austenitic stainless steels and the development of the resulting grain structure. This schematic representation is based on the microstructural results of the present study, as well as on the work of other investigators (Refs. 19, 27, 32). It is used to explain the basic difference in the origin of the solidification grain boundaries resulting from different solidification modes, and the importance of these differences with regard to solidification crack susceptibility.

In a single-phase austenitic solidification mode, austenite is the primary phase and no subsequent phase transformations occur during cooling—Fig. 17A. During this process, the solidification grain boundary develops as Grain A of a given orientation meets with Grain B of a different orientation, bringing about direct contact between two γ grains. In this case, therefore, all solidification grain boundaries are γ-γ boundaries. Austenite is also the primary phase in the austenitic-ferritic solidification mode, where ferrite forms by a eutectic reaction from the melt—Fig. 17B. The amount of ferrite is so low (0 to 2%), however, that it cannot

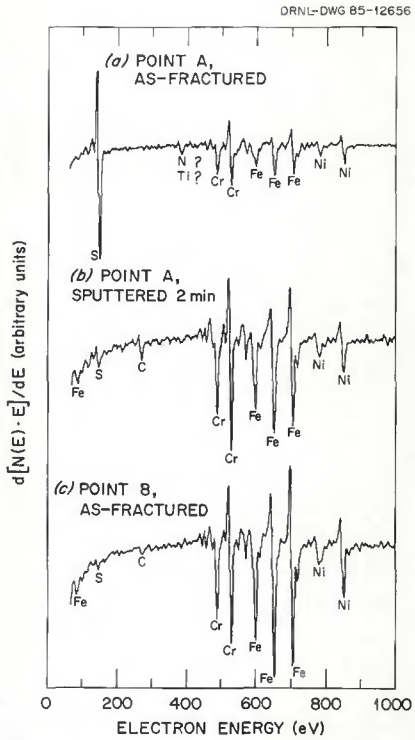

Fig. 14—Auger spectra for the surface in Fig. 13. A and C—Points A and B as-fractured, respectively; B—Point A after 2-min sputtering

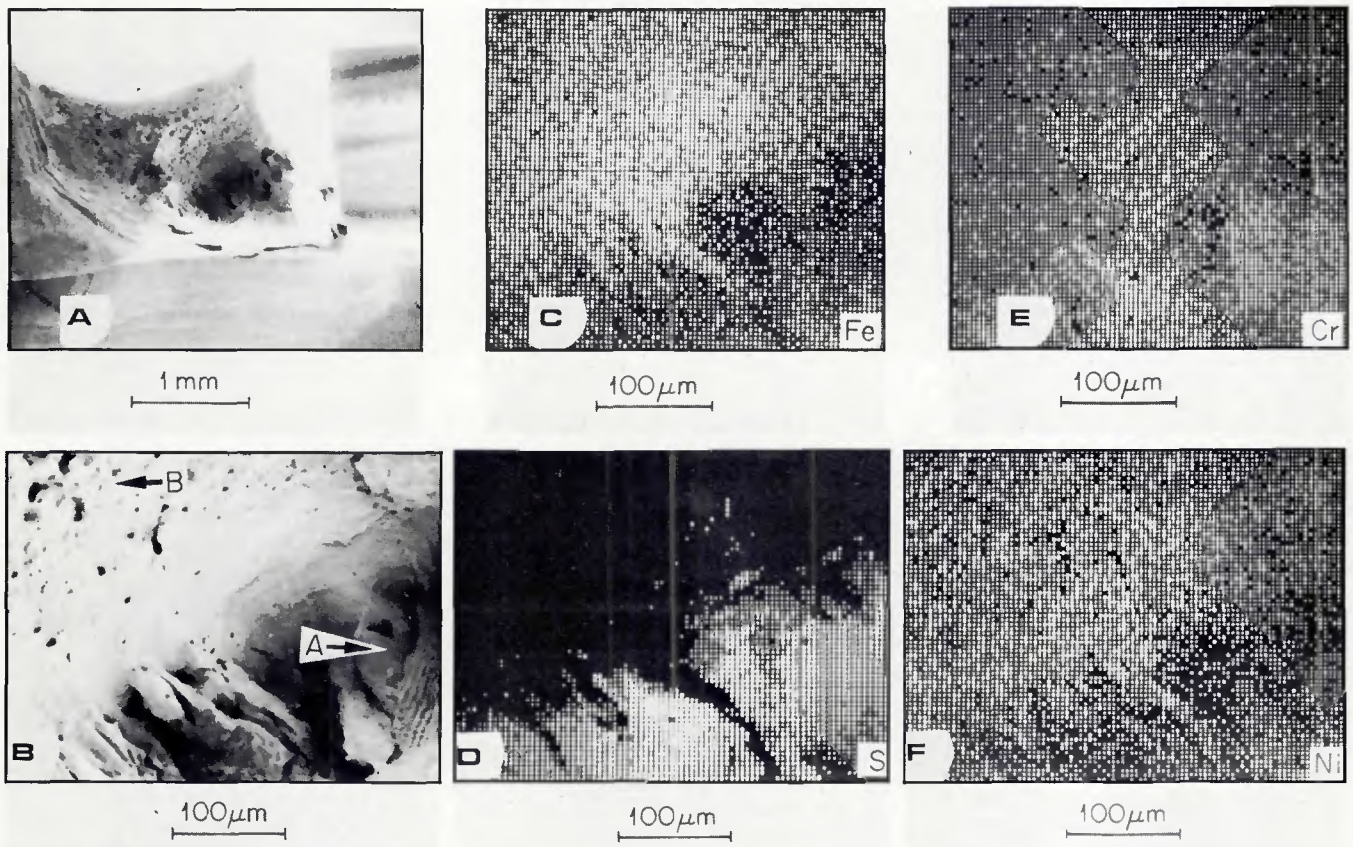

Fig. 15—AES studies on Alloy C weld solidification crack opened inside the Auger electron microscope. A and B—SEM profile of the surface studied; C through F—Fe, S, Cr and Ni AES maps, respectively

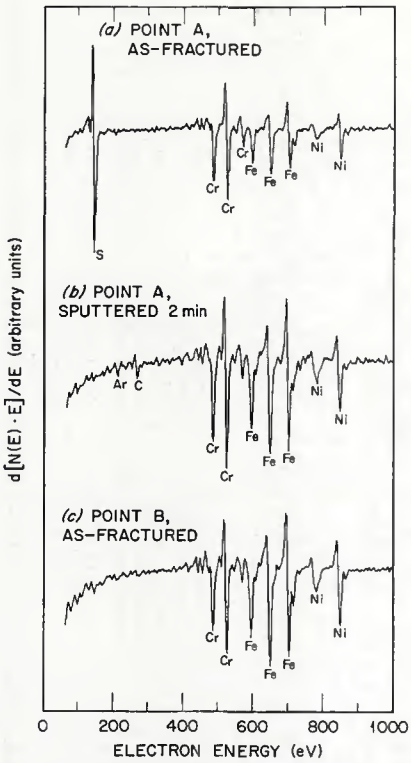

Fig. 16 — AES spectra for the surface in Fig. 15. A and C — Points A and B as-fractured, respectively; B — Point A after 2-min sputtering

prevent the contact between primary austenite grains, and γ-γ grain boundaries develop during solidification in this mode as well. In the presence of a liquid film, the propensity for crack initiation and propagation is very high at these boundaries (Ref. 2). It is generally accepted that the interfacial tensions of γ-γ grain boundaries or δ-δ grain boundaries will be greater than that of δ-γ interphase boundaries (Refs. 41–43). This should result in lower liquid dihedral angles at γ-γ grain boundaries (or complete wetting of γ-γ boundaries) found during the final stages of primary austenitic solidification, rather than at the δ-γ boundaries formed during the final stages of ferritic solidification. The liquid dihedral angle is important because it influences the formation of liquid films on the solidification grain boundaries. If the films form easily (low liquid dihedral angle), relatively larger areas of γ-γ grain boundary may exhibit poor cohesion during the last stages of solidification. In the presence of solidification shrinkage stresses and thermal stresses, the propensity for crack initiation and propagation will be very high at these boundaries. However, if the liquid dihedral angle is large, the last liquid to solidify will tend to form nearly spherical droplets which are relatively isolated from each other and offer limited γ-γ grain boundary areas, over which the grain boundary cohesion will be poor.

The liquid dihedral angle is also influenced by the liquid composition. It is known that harmful impurities, such as sulfur and phosphorus, have lower solubilities in austenite than in ferrite. This will tend to cause the final liquid to be more highly enriched in these harmful impurities for the case of primary austenitic solidification than for the case of primary ferritic solidification. Because these harmful elements are interfacially active, we also expect them to lower the liquid-γ interfacial energy, thus further reducing the liquid dihedral angle for primary austenitic solidification. These low melting impurities will also lower the solidification temperature of the final liquid, further aggravating the cracking.

The AES results of this study support these suppositions about the high content of sulfur in the last liquid to solidify. The solidification crack surfaces were highly enriched in sulfur — Figs. 13–16. The segregation ratio between the top atom layer and the bulk metal was about 2000. We must be careful, when applying these results in practice, however, because sulfur is a surface-active element which has a high tendency to segregate to a free surface at a high temperature. For instance, extensive sulfur segregation to creep cavity surfaces has been found in similar austenitic stainless steels during a heat treatment at a high temperature (Ref. 44). It is possible that the sulfur enrichment on the solidification crack surfaces of the present study was also partly due to free surface segregation after crack formation.

Among the alloys solidifying in the primary austenitic mode, the sulfur contents of the commercial and laboratory heats were at the same level. The concentrations of other minor elements, such as C, Mn, Si, O, N and P, were clearly lower in laboratory heats than the commercial heats. This indicates that these other elements are not playing a major role in hot cracking and that phosphorus is probably the residual element most responsible for hot cracking in alloys solidifying in the primary austenitic mode.

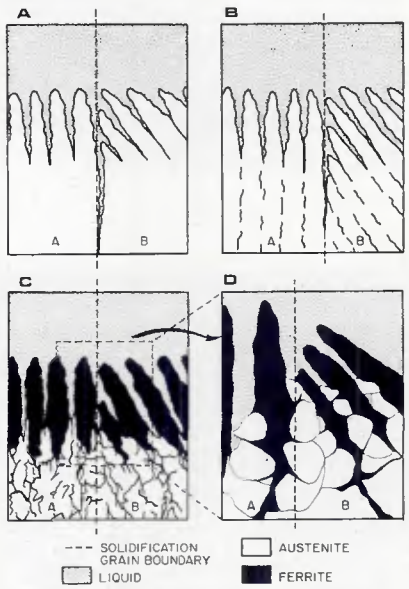

Fig. 17 — Schematic presentation of the development of solidification grain boundary in different modes of solidification. A — Single-phase austenitic; B — Austenitic-ferritic; C — Ferritic-austenitic solidification; D — Enlarged section in C

In the case of the primary ferritic solidification mode (Fig. 17C), ferrite is the primary phase to grow from the liquid. Austenite forms between the dendrites and grows into the ferrite by a three-phase reaction during the last stages of solidification. Because there must be many favorable orientations on the liquid-ferrite boundary for nucleation of the austenite, it is very likely that many austenite grains form on any given ferrite dendrite. Thus, the austenite prevents contact between primary delta ferrite grains and the δ-δ solidification grain boundary, and associated liquid film, as per the previous discussion, is not able to develop. Because many austenite grains form at this critical juncture, the region between two original delta ferrite grains (A and B) is not different than a region between two original delta ferrite dendrites. This means that the propensity for crack initiation and propagation at the grain boundaries formed during primary ferritic solidification is very low, thus inhibiting cracking due to solidification shrinkage stresses and thermal stresses. The differences in the formation mechanisms of solidification grain boundary between different solidification modes is, therefore, suggested to be a new explanation for the enhanced solidification cracking behavior of austenitic stainless steels.

It is known that solidification cracks in austenitic stainless steels are normally intergranular, as seen in Fig. 6A. In the present study, it was found, however, that those few solidification cracks that form in the welds solidified in a primary ferritic mode (Fig. 6B) often can be transgranular. This behavior can also be explained by the different processes of grain boundary development in different solidification modes, as described above. As discussed previously, the region between original delta ferrite grains is not an easier site than an interdendritic region for a crack to initiate in, and cracks, if any, can also be initiated transgranularly. However, for the primary austenitic solidification, high angle γ-γ solidification grain boundaries exist and are the weakest links in the microstructure, and, therefore, cracks formed may form intergranularly.

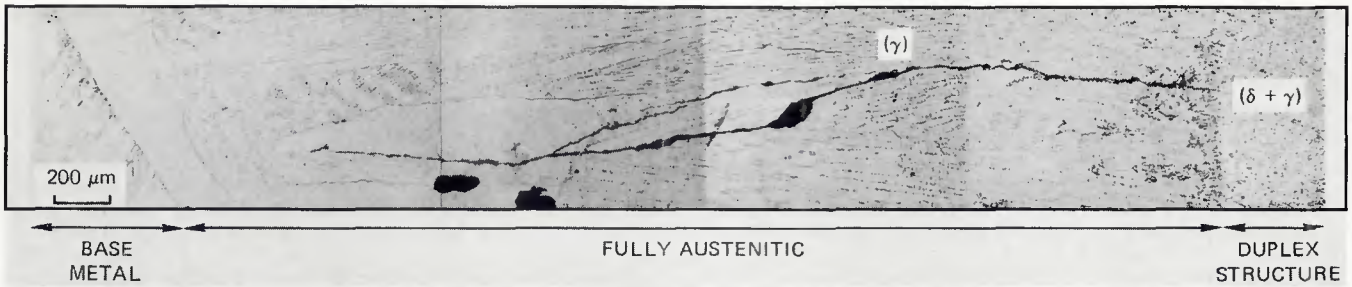

Fig. 18 — A composite picture of austenitic stainless steel weldment, showing cracking in fully austenitic regions and crack arrest in a duplex region

Propagation of Solidification Cracks

It is known that solidification cracks initiate at temperatures close to the solidus. Cracks may propagate over a range of temperatures. However, this range can be even 100° to 200°C wide and be partly below solidus, as confirmed by Arata, *et al.* (Ref. 45).

The nature of the solidification grain boundary also plays an important role in the propagation of solidification cracks (Ref. 27). In the welds solidifying in a primary austenitic mode, grain boundaries are likely to be long, straight γ-γ boundaries, as shown in Figs. 17A and B. Such grain boundaries are expected to provide an easy path for a solidification crack to propagate at lower temperatures. For alloys solidifying in the primary ferritic mode, however, the subsequent $\delta \rightarrow \gamma$ phase transformation, the absence of δ-δ boundaries, and the irregularity of the γ-δ boundaries (Fig. 17C) make the liquid penetration very difficult. In a situation such as this, it is very difficult for a crack to propagate, even if it is nucleated.

Figure 18 is a composite picture of an austenitic stainless steel weld made with Type 308 filler metal and 304L base plates that offers further proof in favor of the above discussions. In regions of the weld solidifying in the primary austenitic mode, very distinct and long grain boundaries are evident. Also, cracks that initiate in these regions, for the reasons discussed previously, propagate along these long, straight (on a macroscopic level) grain boundaries. In regions of the same weld that solidified in a primary ferritic mode, the structure is predominantly duplex $\gamma + \delta$. No distinct grain boundaries were observed. The crack that initiated and propagated through the fully austenitic region gets arrested in the region containing $\gamma + \delta$ duplex structure. This may be due to the absence of δ-δ boundaries or the irregular nature of the solidification grain boundary that becomes part of the δ-δ interphase interface due to migration.

Conclusions

Five ternary Fe-Cr-Ni alloys and five commercial austenitic stainless steel counterparts were evaluated by the Spot-Varestraint test in order to study the formation mechanism of solidification cracking. The results allow the following conclusions to be made:

1. Among the alloys solidifying in primary austenitic mode, there was no remarkable difference between the level of solidification cracking in commercial and high-purity alloy systems. In alloys solidifying in a primary ferritic mode, the high-purity ternary alloy systems showed the least tendency for solidification cracking.

2. The initiation of solidification cracks is controlled by the mode of solidification and the development of solidification grain boundaries. Welds solidifying in a primary austenitic mode tend to develop an extensive liquid film on the solidification γ-γ boundaries leading to an easy initiation of cracks. This may be further aggravated by the presence of low melting solutes such as sulfur. The sulfur content on the solidification crack surfaces has been found to be 2000 times the bulk composition. On the other hand, during the primary ferritic mode of solidification, δ-δ solidification boundaries do not form, and the initiation of a solidification crack is very difficult.

3. The propagation of solidification cracks is also influenced by the mode of solidification and subsequent solid-state transformations. In welds solidifying in the primary austenitic mode, solidification grain boundaries are straight, offering an easy propagation path for cracks. In welds solidifying in the primary ferritic mode, the solidification grain boundaries are eliminated by the three-phase reaction during solidification, leading to more irregular γ-δ phase boundaries which act as crack arresters. Finally, the backfilling of cracks by liquid is found to be easier in the primary ferritic solidification mode than in the primary austenitic mode.

Acknowledgments

Financial support from the Finnish Academy is acknowledged by V. P. Kujanpää. The authors would also like to acknowledge the technical assistance of R. W. Reed in performing the Spot-Varestraint tests, and R. A. Padgett in performing AES analysis. Thanks are also due to Drs. J. M. Vitek and G. M. Goodwin for helpful discussions and review of the manuscript. Research was sponsored by the Division of Materials Sciences, U. S. Department of Energy, under contract DE-AC05-840R21400 with Martin Marietta Energy Systems, Inc.

References

1. Borland, J. C., and Younger, R. N. 1960. Some aspects of cracking in austenitic steels. *British Welding Journal* 71(1):22–60.

2. Hull, F. C. 1967. Effect of delta ferrite on the hot cracking of stainless steel. *Welding Journal* 46(9):399-s to 409-s.

3. Arata, Y., Matsuda, F., and Katayama, S. 1976. Solidification crack susceptibility in weld metals of fully austenitic stainless steel (report) — fundamental investigation on solidification behavior of fully austenitic and duplex microstructures and effect of ferrite on microsegregation. *Transactions of the Japanese Welding Research Institute* 5(2):35–51.

4. Puzak, P. P., Apblett, W. R., and Pellini, W. S. 1956. Hot cracking of stainless steel weldments. *Welding Journal* 35(1):9-s to 17-s.

5. Pellini, W. S. 1952. Strain theory of hot tearing. *Foundry* 80(11):125.

6. Apblett, W. R., and Pellini, W. S. 1954. Factors which influence weld hot cracking. *Welding Journal* 33(2):83-s to 90-s.

7. Borland, J. C. 1960. Generalized theory of super-solidus cracking in welds (and castings). *British Welding Journal* 7(8):508–512.

8. Masumoto, I., and Kutsuma, M. Hot cracking of austenitic steel weld metal. *Japan Welding Journal* 41(11):1306–1314.

9. Astrom, H., Loberg, B., Bengtsson, B., and Easterling, K. E. 1976. Hot cracking and micro-segregation in 18-10 stainless steel welds. *Metal Science* 10(7):225–234.

10. Brooks, J. A., and Lambert, F. J., Jr. 1978. The effects of phosphorus, sulphur and ferrite content on weld cracking of Type 309 stainless steel. *Welding Journal* 57(5):139-s to 143-s.

11. Lundin, C. D., and Chow, C. P. D. November 1983. Hot cracking susceptibility of austenitic stainless steel weld metals. *Welding Research Council Bulletin*, No. 289.

12. Schaeffler, A. L. 1949. Constitution diagram for stainless steel weld metal. *Metals Progress* 56:680–688.

13. DeLong, W. T., Ostrom, G. A., and Szumachowski, E. R. 1956. Measurement and calculation of ferrite in stainless steel weld metal. *Welding Journal* 35(11):521-s to 528-s.

14. DeLong, W. T. 1974. Ferrite in austenitic

stainless steel weld metal. *Welding Journal* 53(7):273-s to 286-s.

15. Lundin, C. D., DeLong, W. T., and Spond, D. F. 1975. Ferrite-fissuring relationship in austenitic stainless steel weld metals. *Welding Journal* 54(8):241-s to 246-s.

16. Lippold, J. C., and Savage, W. F. 1982. Solidification of austenitic stainless steel weldments: part III—the effect of solidification behavior on hot cracking susceptibility. *Welding Journal* 61(12):388-s to 396-s.

17. Masumoto, I., Tamaki, K., and Kutsuna, M. 1972. Hot cracking of austenitic steel weld metal. *Journal of JWS* 41(11):1306-1314, Brutcher Transl. 8965/1973.

18. Thier, H. 1975. Schweissen Hochlegierten Stahle. *DVS-Berichte* 33:69-75.

19. Arata, Y., Matsuda, F., and Katayama, S. 1976. Fundamental investigation of solidification behaviour of fully austenitic and duplex microstructures and effect of ferrite on microsegregation. *Transact. JWRI* 5(2):35-51.

20. Kujanpää, V., Suutala, N., Takalo, T., and Moisio, T. 1979. Correlation between solidification cracking and microstructure in austenitic and austenitic-ferritic stainless steel welds. *Welding Research International* 9(2):55-76.

21. Gooch, T. G., and Honeycombe, J. 1980. Welding variables and microfissuring in austenitic stainless steel weld metal. *Welding Journal* 79(8):233-s to 240-s.

22. Kujanpää, V. 1983. Weld defects in austenitic stainless steel sheets—effect of welding parameters. *Welding Journal* 62(2):45-s to 52-s.

23. Dixon, B. 1981. Weld metal solidification cracking in ferritic steels—a review. *Australian Welding Journal* 26(4):23-30.

24. Kujanpää, V., Suutala, N., Takalo, T., and Moisio, T. 1980. Solidification cracking—estimation of the susceptibility of austenitic and austenitic-ferritic stainless steel welds. *Metal Construction* 12(6):282-285.

25. Kujanpää, V. 1985. Effect of steel type and impurities in solidification cracking of austenitic stainless steel welds. *Metal Construction* 17(1):40R-46R.

26. Matsuda, F., Nakagawa, H., Katayama, S., and Arata, Y. 1982. Solidification crack susceptibility in weld metals of fully austenitic stainless steels. Report 6: effect of La or REM addition on solidification crack resistance. *Transact. JWRI* 11(1):79-94.

27. Brooks, J. A., Thompson, A. W., and Williams, J. C. 1984. A fundamental study of the beneficial effects of delta ferrite in reducing weld cracking. *Welding Journal* 63(3):71-s to 83-s.

28. Hemsworth, B., Bonizewski, T., and Eaton, N. F. 1969. Classification and definition of high temperature welding cracks in alloys. *Metal Construction and British Welding Journal* 1(2):5-16.

29. Goodwin, G. M. 1968. The effect of minor elements on the hot cracking tendencies of Inconel 600. Ph.D. thesis, Rensselaer Polytechnic Institute, Troy, N. Y.

30. Savage, W. F., and Lundin, C. D. 1965. The Varestraint test. *Welding Journal* 44(10):433-s to 442-s.

31. Davis, L. E., *et al.* 1976. *Handbook of Auger Electron Spectroscopy,* 2nd ed. Physical Electronics Industries, Inc., Eden Prairie, Minn.

32. Suutala, N., Takalo, T., and Moisio, T. 1979. Relationship between microstructure and solidification in austenitic stainless steel welds. *Met. Trans.* 10A(4):512-514.

33. David, S. A., Goodwin, G. M., and Braski, D. N. 1979. Solidification behavior of austenitic stainless steel filler metals. *Welding Journal* 58(11):330-s to 336-s.

34. Takalo, T., Suutala, N., and Moisio, T. 1979. Austenitic solidification mode in austenitic stainless steel welds. *Met. Trans.* 10A(8):1173-1181.

35. Suutala, N., Takalo, T., and Moisio, T. 1979. Single-phase ferritic solidification mode in austenitic-ferritic stainless steel welds. *Met. Trans.* 10A(8):1183-1190.

36. Suutala, N., Takalo, T., and Moisio, T. 1980. Ferritic-austenitic solidification mode in austenitic stainless steel welds. *Met. Trans.* 11A(5):717-725.

37. David, S. A. 1981. Ferrite morphology and variations in ferrite content in austenitic stainless steel welds. *Welding Journal* 60(4):63-s to 71-s..

38. Hammar, O., and Svensson, U. 1979. Influence of steel composition on segregation and microstructure during solidification of austenitic stainless steels. *Proc. Conf. Solidification and Casting of Metals,* pp. 401-410, The Metals Society, London, England.

39. Suutala, N. 1982. Effect of manganese and nitrogen on solidification mode in austenitic stainless steel welds. *Met. Trans.* 13A(12):2121-2130.

40. Suutala, N. 1983. Effect of solidification conditions on the solidification mode in austenitic stainless steels. *Met. Trans.* 14A(2):191-197.

41. Smith, C. S. 1948. Grains, phases, and interfaces: an interpretation of microstructure. *Trans. American Institute of Mining and Metallurgical Engineers* 175:15-51.

42. Smith, C. S. 1952. *Interphase Interfaces, Imperfections in Nearly Perfect Crystals,* pp. 377-401. John Wiley and Sons, New York, N. Y.

43. Taylor, J. W. 1958. An evaluation of interface energies in metallic systems. *Journal Institute of Metals* 86:456-463.

44. White, C. L., Schneibel, J. H., and Yoo, M. H. 1984. Sulfur and antimony segregation to creep cavity surfaces in Ni and an FCC Fe-Ni-Cr Alloy. *Proc. Conf. Creep and Fracture of Engineering Materials and Structures,* eds. B. Wilshire and D. R. J. Owen, pp. 347-358. Pineridge Press, Swangea, England.

45. Arata, Y., *et al.* 1977. Solidification crack susceptibility in weld metals of fully austenitic stainless steels. *Trans. JWRI* 6(2):37-46.

WRC Bulletin 314
May 1986

Bolted Flanged Connections with Full Face Gaskets
By A. E. Blach, A. Bazergui and R. Baldur

A flange type commonly called "flat-face" flange has been used in certain classes of bolted flanged connections for many years, yet no code rules exist to cover this class of flanged connections. This paper analyzes the behavior of gaskets and flanges in such a connection and gives design formulas which follow the philosophy of the present code rules for bolted flanged connections. A numerical example is included which shows the application of the design formulas and compares results obtained with values from strain gage measurements on a pressure vessel of the same size.

Publication of this report was sponsored by the Subcommittee on Bolted Flanged Connections of the Pressure Vessel Research Committee of the Welding Research Council. The price of WRC Bulletin 314 is $12.00 per copy, plus $5.00 for postage and handling. Orders should be sent with payment to the Welding Research Council, Ste. 1301, 345 E. 47th St., New York, NY 10017.